Numerical Method for Computing Nonlinear, Time Dependent, Buoyant Circulation of Air in Rooms*

Abstract: A method is described which solves the dynamic equations for air circulation at Grashof numbers that are in the range of environmental temperatures of rooms. Previous two-dimensional computation techniques were limited to $G \approx 10^5$ but environmental conditions require $G \approx 10^{12}$. The higher Grashof numbers become calculable through the design of a mixed system of nonlinear difference equations which has purely leading-phase-error properties. In addition provision is made for nonlinear stability by explicitly programming cross derivative terms in lieu of employing "time splitting." The isotropic behavior achieved through time splitting is retained by the system of difference equations. Details of the required algorithms are included.

Introduction

In the past decade numerous advances have been made in the use of numerical means to solve coupled nonlinear partial differential equations. The methods for obtaining solutions fall roughly into two categories: 1) Expansion methods which make use of orthogonal polynomials, and 2) finite difference methods. The former was used by Poots [1] and the latter by Wilkes [2] for the particular problem of interest here. The two methods were about equally successful for the solutions reported by these authors. Comparable solutions were obtained for the problems of buoyant fluid flow in a two-dimensional enclosure with vertical walls at a fixed temperature difference and with horizontal walls that were either insulated or had a fixed temperature that varied linearly between the upright walls. These successes were important ones and led to the hope that the methods could readily be extended beyond the range of parameters of those studied into the practical problems of everyday engineering experience, in particular to the study of air circulation at environmental room temperatures or under fire conditions.

Both methods do possess the potential of providing solutions to such problems. Currently, the greatest emphasis is on finite difference methods because they may be applied in a straightforward manner if sufficiently accurate algorithms are known. Unfortunately, such algorithms have been slow in realization. Here we have

Our primary objectives here are to outline the numerical methods and to give details of the required algorithms. The general procedure of finite difference computation using the vorticity and streamfunction as field variables is fairly well established [3–5]. Also, the evolution of thought on requirements relative to reduction of phase error, which is the primary cause of computational noise, has been documented [6, 7]. The additional modifications of the basic algorithms that are pertinent for the success of high-Grashof-number calculations are emphasized in the present paper.

As a result of these efforts toward minimizing numerical noise and numerical damping, the two-dimensional computation can to some extent be carried out up to Grashof numbers of 10^{12} . At these high values there are uncertainties about the magnitude of viscosity and heat transfer coefficients relative to truncation errors. Further, very small time increments are required for computation. Hence the limiting calculation of infinite Grashof number would not be a reasonable one.

utilized higher order approximations that depend upon flow direction. This is essential in order that detail may be maintained without introduction of noise components that are of numerical origin. The nature of the flow in the rectangular enclosure is such that the common weaknesses of nonlinear difference approximations are very pronounced. Thus although the geometrical situation is fairly simple, it provides a crucial test of the methods.

^{*} An earlier version of this paper was presented at the First Symposium on the Use of Computers for Environmental Engineering Related to Buildings, National Bureau of Standards, Gaithersburg, Md., December 1, 1970.

Because turbulence is surely a factor in the real world, the present calculations using molecular coefficients should be regarded as idealizations. This does not mean that they are of little value. On the contrary, we can analyze the flow behavior and then explain the flow features and why they occur. Further, gross properties of the flows can be given within the framework of the idealization. With this information it should be possible, with the help of experiments, to determine where discrepancies occur between observation and computation. Information so obtained is pertinent to modeling efforts where parameters must be assigned to turbulent diffusion and heat transport.

It should also be noted that our two-dimensional results will have to be contrasted with three-dimensional results when these become available. We have chosen to solve two-dimensional problems for large values of the parameter rather then to attempt the far more difficult task of programming for three dimensions, where one has promise of results for only very slow viscous flows in terms of present computer capabilities. The present approach would tend to imply that three-dimensional laminar instabilities have little to do with gross behavior if the experiment is designed to provide two-dimensional flow. This implication is known to be wrong in regard to flow features but may not be seriously wrong in terms of heat transfer measurements.

Governing equations and problem description

The conservation equations to be solved in a two-dimensional rectangular region are:

$$Mass: \qquad \frac{\partial u}{\partial x} + \frac{\partial v}{\partial y} = 0, \qquad (1)$$

Momentum:
$$\frac{\partial u}{\partial t} + u \frac{\partial u}{\partial x} + v \frac{\partial u}{\partial y} = -\frac{1}{\rho_0} \frac{\partial P}{\partial x} + v \nabla^2 u$$
,

(2)

$$\frac{\partial v}{\partial t} + u \frac{\partial v}{\partial x} + v \frac{\partial v}{\partial y} = -\frac{1}{\rho_0} \frac{\partial P}{\partial y}$$
$$-g \left(\frac{T - T_0}{T_0}\right) + \nu \nabla^2 v, \qquad (3)$$

Energy:
$$\frac{\partial T}{\partial t} + u \frac{\partial T}{\partial x} + v \frac{\partial T}{\partial y} = \kappa \nabla^2 T. \tag{4}$$

Here u and v are the respective velocity components in the x and y directions. The thermodynamic variables ρ , P, and T are the density, pressure and temperature, respectively. The subscript 0 indicates constant reference values to be defined. The symbols ν , κ and g are the kinematic viscosity, thermometric conductivity and gravitational constant.

Numerical computation is carried out using the vorticity and streamfunction. We define

$$\omega = \frac{\partial v}{\partial x} - \frac{\partial u}{\partial y} \tag{5}$$

and

$$u = \frac{\partial \psi}{\partial v}, \qquad v = -\frac{\partial \psi}{\partial x}. \tag{6}$$

Thus (1) is satisfied identically by (6), (5) becomes

$$\frac{\partial^2 \psi}{\partial x^2} + \frac{\partial^2 \psi}{\partial y^2} = -\omega, \tag{7}$$

and P can be eliminated from (2) and (3) yielding the vorticity equation

$$\frac{\partial \omega}{\partial t} + \frac{\partial u\omega}{\partial x} + \frac{\partial v\omega}{\partial y} = -\frac{g}{T_0} \frac{\partial T}{\partial x} + \nu \nabla^2 \omega. \tag{8}$$

Our system of computation equations are then (7), (8), (4) and the definitions (6).

We take x as the horizontal coordinate and impose the boundary conditions for a square enclosure as

$$u = v = 0, T = T_1$$
 at $x = 0$ for $0 \le y \le d$,
 $u = v = 0, T = T_0$ at $x = d$ for $0 \le y \le d$,
 $u = v = 0$ at $y = 0, d$ for $0 \le x \le d$,
 $T = T_1 - x(T_1 - T_0)/d$

at
$$y = 0, d$$
 for $0 < x < d$.

It is more convenient to deal numerically in terms of the dimensional variables because of the physical interpretation and the number sizes encountered in numerical solution. Following Poots, we use the nomenclature $\sigma = \nu/\kappa$ as the Prandtl number and $A = \sigma G = (T_1 - T_0)$ $gd^3/T_0\kappa\nu$ for the Rayleigh and Grashof numbers A and G, respectively.

While numerous gross properties could be evaluated to lend understanding to the flows, we here consider the dimensionless heat transfer for comparison with results by Poots and Wilkes. Heat transmission through the cold vertical boundary is not the total heat transmission but is the value given by Poots. Numerically, one must also include the convection flux because the discrete description requires it. For the square region considered we define the Nusselt number

$$N = \frac{\kappa \int_0^d \frac{\partial T}{\partial x} dy + \int_0^d uT dy}{\kappa (T_1 - T_0)}.$$

The total heat transmission can be evaluated only by having the end points of the integration correspond to x = d/2 and y = 0,d. Nevertheless, for comparison

187

purposes we also measure the transmission at x = 0 with integration limits y = 0,d.

Numerical approximations

We now describe the nonlinear approximation method that was required for the success of the given calculations. For completeness we shall first outline all the numerical approximations, postponing the details of the convective flux method for later discussion.

For small values of A or G it may be advisable to begin calculation with no flow and an initially prescribed linear horizontal temperature variation inside the fluid region. If A is small, steady-state results are of primary interest and computation time may be preserved by relay type calculations, always using steady-state results from lower values of A to proceed to higher values. However, beyond $A = 10^6$ the solutions are unsteady, e.g., $A = 10^6$, $\sigma = 0.1$ gives an oscillating solution. While it is always useful to begin with an approximate solution to the expected solution at late time, it is more reasonable to start calculation at high values of A with internal temperatures specified to be everywhere the mean of the given wall temperatures. If the initial interior temperature is specified to be that of the low-temperature wall, much computation would be required to approach true late-time conditions. In all cases reported here, we began with the temperature field at the mean wall-temperature value. The streamfunction and vorticity were prescribed to be everywhere zero initially.

With all field values given at the time t=0 we proceed by updating the temperature field toward ultimate prescription of field values $T_{i,j}^n = T(i\Delta x, j\Delta y, n\Delta t)$ for n=1. Through convective flux computation we first obtain everywhere

$$\tilde{T}_{i,j} = T^{0}_{i,j} + \frac{\Delta t}{\Delta x} (F^{0}_{i-\frac{1}{2},j} - F^{0}_{i+\frac{1}{2},j}) + \frac{\Delta t}{\Delta y} (F^{0}_{i,j-\frac{1}{2}} - F^{0}_{i,j+\frac{1}{2}}),$$
(10)

where F is the flux at half-cell distances from the point (i, j). Using everywhere the tentative values (except for fixed values at the boundaries) we add the conduction contribution to complete the update of T. Thus

$$T_{i,j}^{1} = \tilde{T}_{i,j} + \frac{\kappa \Delta t}{(\Delta x)^{2}} (\tilde{T}_{i+1,j} - 2\tilde{T}_{i,j} + \tilde{T}_{i-1,j}) + \frac{\kappa \Delta t}{(\Delta y)^{2}} (\tilde{T}_{i,j+1} - 2\tilde{T}_{i,j} + \tilde{T}_{i,j-1}).$$
(11)

The use of tentative updated values in the conduction calculation provides for less restrictive conditional stability of this explicit difference equation. This has been suggested in the work of Marchuk [8] and has been observed empirically in the present calculations. Through this procedure the stability condition

$$\kappa \Delta t / \min \left[(\Delta x)^2, (\Delta y)^2 \right] < \frac{1}{4}$$
 (12)

is strictly applicable. For small A, a more stringent condition would otherwise be necessary. For A large, the convection condition $u\Delta t/\Delta x \leq 1.0$ governs the time-step size and the use of updated (\tilde{T}) values would not be necessary.

At this stage one proceeds similarly with the vorticity equation, first obtaining

$$\tilde{\omega}_{i,j} = \omega_{i,j}^{0} + \frac{\Delta t}{\Delta x} \left(H_{i-\frac{1}{2},j}^{0} - H_{i+\frac{1}{2},j}^{0} \right) + \frac{\Delta t}{\Delta y} \left(H_{i,j-\frac{1}{2}}^{0} - H_{i,j+\frac{1}{2}}^{0} \right), \tag{13}$$

where H is the vorticity flux analogous to F of (10). Here two tentative updates are necessary because of the buoyancy term. For the diffusion update we write

$$\omega_{i,j}^{*} = \tilde{\omega}_{i,j} + \frac{\nu \Delta t}{(\Delta x)^{2}} (\tilde{\omega}_{i+1,j} - 2\tilde{\omega}_{i,j} + \tilde{\omega}_{i-1,j}) + \frac{\nu \Delta t}{(\Delta \nu)^{2}} (\tilde{\omega}_{i,j+1} - 2\tilde{\omega}_{i,j} + \tilde{\omega}_{i,j-1}).$$
(14)

Finally the buoyancy contribution gives the complete update of ω :

$$\omega_{i,j}^{1} = \omega_{i,j}^{*} + \frac{g\Delta t}{2T_{0}\Delta x} (T_{i+1,j}^{1} - T_{i-1,j}^{1}). \tag{15}$$

Note that the values obtained in (11) are necessary in (15). If in (15) the old-times values were used, numerical instability would result. This follows from a simple linear analysis which we do not include here.

With T and ω both obtained for new times we next consider the streamfunction field. Simultaneous solution of all net points is required to satisfy

$$\frac{\psi_{i+1,j}^{1} - 2\psi_{i,j}^{1} + \psi_{i-1,j}^{1}}{(\Delta x)^{2}} + \frac{\psi_{i,j+1}^{1} - 2\psi_{i,j}^{1} + \psi_{i,j-1}^{1}}{(\Delta y)^{2}} = -\omega^{1}.$$
(16)

Because of the simplicity of the boundary conditions on ψ a direct method may readily provide solution. We have here made use of a program developed by Bunemann [9], whose method involves cyclic matrix reduction in two directions. It is applicable to an enclosed rectangular region with zero value specified for ψ at the boundaries. The program is fast, accurate to computer roundoff, and compact. It is estimated that, to attain equal accuracy, an iterative method would have taken more than ten times as much computation.

The final step in computation of the field variables, to have a complete solution at the advanced time step, is to apply no-slip conditions at the walls, i.e., obtain boundary vorticity values. The approximations here used are

$$\omega_{0,i}^{1} = -2(\psi_{1,i}^{1} - \psi_{0,i}^{1})/(\Delta x)^{2}
\omega_{I,i}^{1} = 2(\psi_{I,i}^{1} - \psi_{I-1,i}^{1})/(\Delta x)^{2}
\omega_{i,0}^{1} = -2(\psi_{i,1}^{1} - \psi_{i,0}^{1})/(\Delta y)^{2}
\omega_{i,J}^{1} = 2(\psi_{i,J}^{1} - \psi_{i,J-1}^{1})/(\Delta y)^{2},$$
(17)

where 0 refers to left or lower boundary and I and J refer to right and upper boundaries, respectively. The equations (17) may readily be derived from (16). Corner values of ω are always zero as implied by successive use of appropriate parts of (17).

Stability of the explicit form of solution is tested at all time steps and provision is made to double or halve the time step. If the larger of $|u| \Delta t/\Delta x$ and $|v| \Delta t/\Delta y$ is less than 0.4, the time step is doubled. If the larger of $|u| \Delta t/\Delta x$ and $|v| \Delta t/\Delta y$ is greater than 1.0, the time step is cut in half. Applying these conditions along with (12) maintains stability throughout the solution process. While an initial estimate of Δt is not required by this procedure some early-time rapid adjustment of Δt does occur for large A. In these cases a maximum early time Δt should be used for the first several time steps because a very large Δt is implied by the stability conditions. Equation (15) is overstable and no test is necessary for this part of the procedure.

With a view of the over-all procedure we now give further consideration to F of Eq. (10) or H of Eq. (13). Both F and H are, in computation, handled by the same program. Prior experience led to fourth-order, onedimensional approximations for F on the assumption that "time splitting" methods would be used to provide isotropic behavior relative to the finite lattice. "Time splitting" is here used throughout to mean the convection process which involves computation of tentative values through the addition of horizontal flux contributions followed by addition of vertical flux contributions. Here the latter computation makes use of the tentative values derived from the horizontal additions. In a linear sense, time splitting results in the inclusion of diagonal values of the field variable such that truly two-dimensional flow is treated. It is an efficient way to obtain isotropic behavior since without time splitting or some equivalent procedure one may, in the extreme case, obtain instability in the flow direction simultaneous to numerical diffusion transverse to the flow direction. Often these two effects can hold the numerical computation in check but the results may be badly in error, since distortion occurs here even if the flow is uniform but not along the coordinate axes.

In two dimensions then we must in some sense bring in mesh values of the field variables that are diagonally distributed relative to the coordinate directions at (i, j).

Unfortunately, while time splitting is an efficient procedure to use, it has been found that a new type of instability can occur. This instability is slow and occurs only in nonlinear cases. In the given problem a vortex originating from buoyant effects may grow in intensity in a nonphysical manner. This difficulty is not very different from that of using nonconservative difference methods. It is perhaps less severe, since its degree of severity depends upon the nonlinearity of the problem and the amplitude characteristics of the approximation. The difficulty has its origin in an inconsistency that occurs in the velocity values that are effectively present in the implied cross differences. Since the cross derivatives *are* implied through time splitting, this short-coming goes unnoticed until the slow-growing instability occurs.

Here the difficulty is circumvented by explicitly programming cross derivatives as required to provide the linear equivalent of time splitting procedures. By so doing the linear stability conditions are maintained and the inconsistencies in velocity values are avoided. If one expands the time splitting equations into a single step the cross differences will appear. Using these terms as a guide, final layout of conservative expressions are developed from a Taylor series expansion [10]. Consider, for example,

$$T^{n+1} = T^n + \Delta t \left(\frac{\partial T}{\partial t} \right) + \frac{(\Delta t)^2}{2} \left(\frac{\partial^2 T}{\partial t^2} \right) + \cdots . \quad (18)$$

Because we are numerically separating convection and conduction, we take

$$\frac{\partial T}{\partial t} = -\frac{\partial uT}{\partial x} - \frac{\partial vT}{\partial y}. (19)$$

If we use (19) to obtain the second time derivative of (18) and drop derivatives of velocity with respect to time, we obtain

$$\frac{\partial^{2} T}{\partial t^{2}} = \frac{\partial}{\partial x} \left(u^{2} \frac{\partial T}{\partial x} + uv \frac{\partial T}{\partial y} \right)
+ \frac{\partial}{\partial y} \left(uv \frac{\partial T}{\partial x} + v^{2} \frac{\partial T}{\partial y} \right).$$
(20)

Here the (uv) terms are the first cross terms that must be explicitly programmed rather than implied as in time splitting. The (uv) term has two parts, one part is regarded as a skew flow correction to the flux in the xdirection, the other part as a skew flow correction to the flux in the y direction. With similar expansion of (18) to eighth order, all cross derivatives required for fourthorder accuracy in space are included. The additional terms involving orders higher than fourth in time provide

189

for a stability in two dimensions that is not restricted beyond that of the one-dimensional counterpart of the approximation. Proper combination of spatial differences, so that they enter the computation recursively, can lead to reasonably fast computation. The fourth-order difference method is given in the Appendix.

We justify dropping velocity derivatives from the expressions like Eq. (20) in that local averages are used which apply over a spatial domain consistent with the numerical stability conditions. The local averages have the additional merit that they preserve continuity. A more elaborate approach to this problem would be expected to have difficulty in this connection.

One further consideration in the convective approximation is phase distortion. It is particularly pertinent to the problem at hand since the usual difference methods would quickly lead to meaningless results for $A > 10^7$. It is essential to success of such calculations to have leading phase errors (i.e., to have short waves travel faster than they should, rather than slower) and these errors should be small. Upstream approximations may be linked through different magnitudes of $\alpha = u\Delta t/\Delta x$. Here we have used a combined fourth-order upstream and central approximation (flow direction must here also be tested) for $0.5 \le |\alpha| \le 1.0$. For $0.09 \le |\alpha| < 0.5$ the fourth-order upstream approximation alone is used. If $|\alpha| < 0.09$ a second-order upstream approximation is employed. Central approximations are used only for flow away from solid boundaries if data points for upstream calculation are not available. In these latter instances lagging phase errors do not lead to noise. The use of second-order upstream approximations for $|\alpha|$ 0.09 has to do with an anomaly in fourth-order characteristics not present in second-order ones. The above procedure, of course, is not the only one that may be used. In the given case it was the most expedient on the basis of available data on phase properties of the methods (see Ref. 7).

The choice of nonlinear difference methods also included consideration of amplitude properties to limit numerical damping. A rough estimate of this damping compared with the viscous damping indicates that they become comparable when $A \approx 10^8$ for say a wavelength of $\lambda = 6\Delta x$. Nevertheless since the damping effects enter through different mechanisms, distinctions in the time development continue to be observable between $A = 10^{11}$ and $A = 10^{12}$. We do not currently know whether the distinction is adequate at these high values of A but intuitively one also expects very little difference.

The improved amplitude characteristics of fourth order best justify the increase in computation time that would be required for a given number of mesh points of the grid (65×65) in the present application). We estimate that $\frac{3}{2}$ as many points in one dimension would be required

for equal accuracy for second-order methods. This means a computer time increase of $(\frac{3}{2})^3$ because of the stability condition and two dimensions. Since the increased complexity of fourth order produces a factor roughly inverse to this, the nonlinear computation alone would not justify programming for fourth order. However since the nonlinear computation is $\frac{1}{3}$ or less of the over-all computation a pessimistic estimate is that fourth-order computation provides a factor of 2 increase in computation speed (since increased accuracy of the elliptic and parabolic parts of the equations is not needed). Also more than twice as much output data would have to be processed.

Flow behavior

At the time of this writing we have computed several cases to give an over-all view of how flows vary with Rayleigh number and Prandtl number. Computations have been made for $A=10^4$ through $A=10^{12}$ at intervals of a factor of 10 with $\sigma=1.0$. For even powers of A, runs were also made for $\sigma=10.0$ and $\sigma=0.1$. From these computations the flows can be classed roughly into three groups:

- 1) Steady-state flows ($G \lesssim 10^7$);
- 2) Transition flows, unsteady and highly variable in behavior ($10^7 \lesssim G \lesssim 10^9$); and
- 3) Single-circulation, high-Grashof-number flows ($10^9 \lesssim G < 10^{13}$).

The steady-state flows are also single-circulation flows characterized by the presence of a vertical temperature gradient in the central region of the enclosure but little horizontal temperature gradient. The temperature gradients increase strongly near the walls. This type of behavior is illustrated in the steady solution of $A = 10^5$, $\sigma = 1.0$ of Fig. 1. Figures 1(a), 1(b) and 1(c) are contour maps. Figures 1(d), 1(e) and 1(f) are perspective views corresponding to Figs. 1(a), 1(b) and 1(c), respectively.

In the transition flows (Fig. 2) the variable behavior includes sinusoidal behavior at the low values of G. Midtransition flows deviate from sinusoidal to include random occurrences of buoyant plumes along the horizontal boundaries. In the upper transition flows randomness is increased, and boundary layer entrainment leads to counter circulations mixed with buoyant circulations. Figure 2 is an example of upper transition range flow. Again perspective views of Figs. 2(a), 2(b), and 2(c) are given in Figs. 2(d), 2(e) and 2(f).

Members of the last group are classed together because visually they exhibit little difference in behavior. A single circulation (in the square region) is the main feature and is common to the whole group. The interior fluid is essentially isothermal at the mean temperature and vorticity is relatively absent there. One can describe these flows as having an inner core of nearly ideal fluid

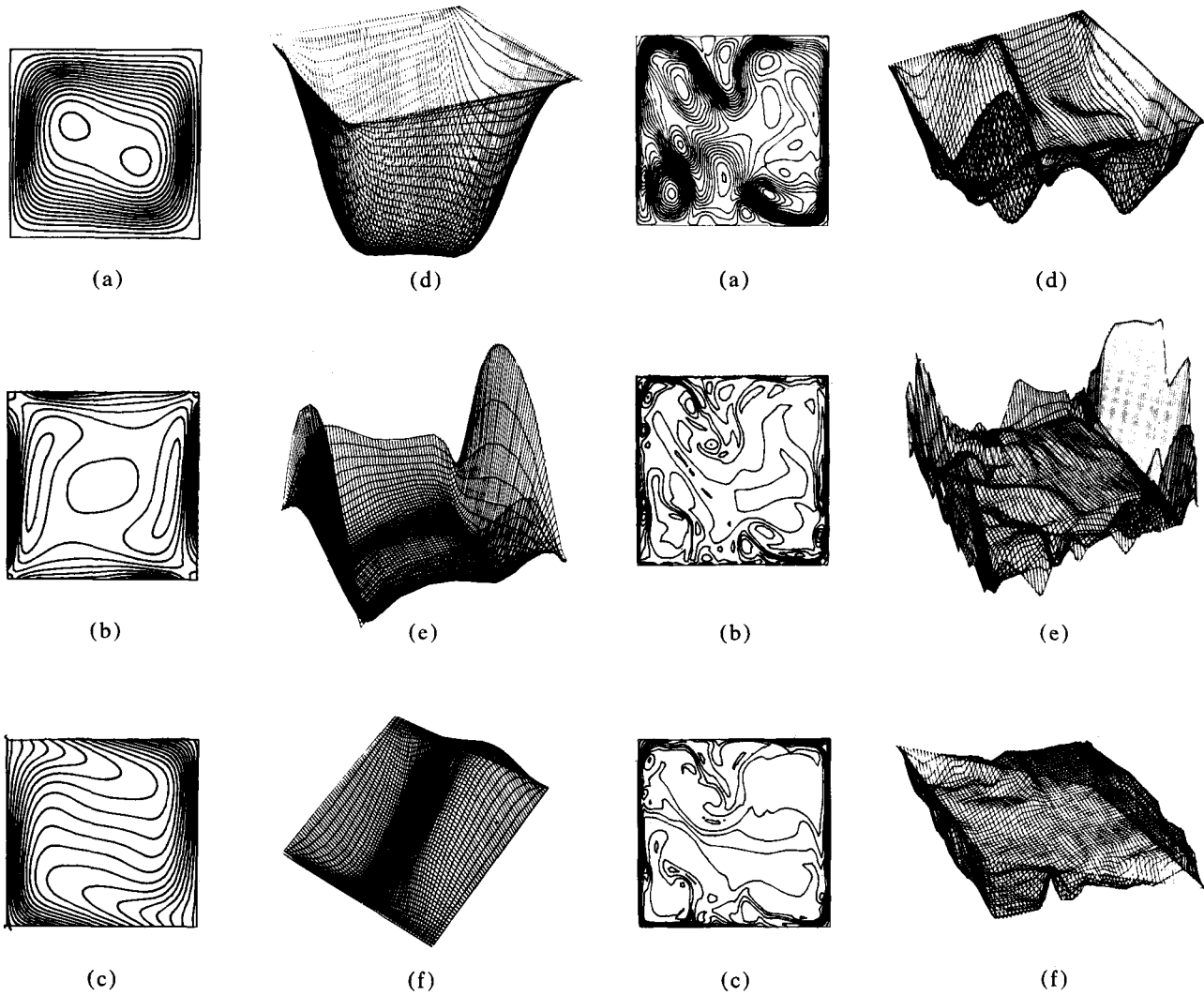


Figure 1 Steady-state flows. (a) Steady streamline solution for $A=10^5$, $\sigma=1.0$. The plot increment $\Delta\psi=0.05$ ft²/sec. $\psi = 0$ at the boundary and 0.025 at the first contour from the boundary. (b) Contours of constant vorticity for $A = 10^5$, $\sigma = 1.0$. The plot increment $\Delta \omega = 0.2/\text{sec}$. The minimum displayed contour value is -0.5 and is the inner contour of the two symmetric extremals. ω maximum at the wall is 2.47. (c) Isotherms for $A = 10^5$, $\sigma = 1.0$. The plot increment is $\Delta T = 0.5$ °F for the over-all wall temperature difference $T_1 - T_0 = 10.0$. (d) Perspective view of Fig. 1(a). Note that the corner nearest the observer is the lower left corner of Fig. 1(a). (e) Perspective view of Fig. 1(b). The corner nearest the observer is the lower left of Fig. 1(b). The boundary layer vorticity is the dominant feature. (f) Perspective view of Fig. 1(c). The corner nearest the observer is the lower right of Fig. 1(c).

Figure 2 Transition flows. (a) Late-time streamline solution for $A=10^\circ$, $\sigma=1.0$. The plot increment $\Delta\psi=0.02$ ft²/sec. The separation streamline $\psi=0$ is given and is the reference contour. (b) Vorticity contours corresponding to Fig. 2(a). $\Delta\omega=0.75/{\rm sec.}$ ω maximum at the wall is 12.9. (c) Isotherms corresponding to Fig. 2(a) $\Delta T=0.5^\circ {\rm F.}$ (d) Perspective view of Fig. 2(a). The corner nearest the observer is the lower left of Fig. 2(a). The dominant positive excursion is the counter rotating vortex in the lower left corner. (e) Perspective view of Fig. 2(b). The corner nearest the observer is the lower left of Fig. 2(b). Boundary layer vorticity at the vertical walls is here the dominant feature. (f) Perspective view of Fig. 2(c). The corner nearest the observer is the lower left of Fig. 2(c).

flow and a highly variable boundary layer behavior. The thermal and velocity boundary layers are thin but corner regions are involved in the flow related to these layers. In Fig. 3 we include an example from this group.

Returning now to Fig. 1 we consider the steady-state flows in more detail. In Fig. 1(a) the streamlines of the

flow are given. The highest speeds, as expected, are of flow near the vertical boundaries, while the flow near the center is slow. The separated centers of circulation are in the same direction of rotation. They occur because of two regions of buoyant vorticity associated with the heated and cooled vertical walls. They are separated by

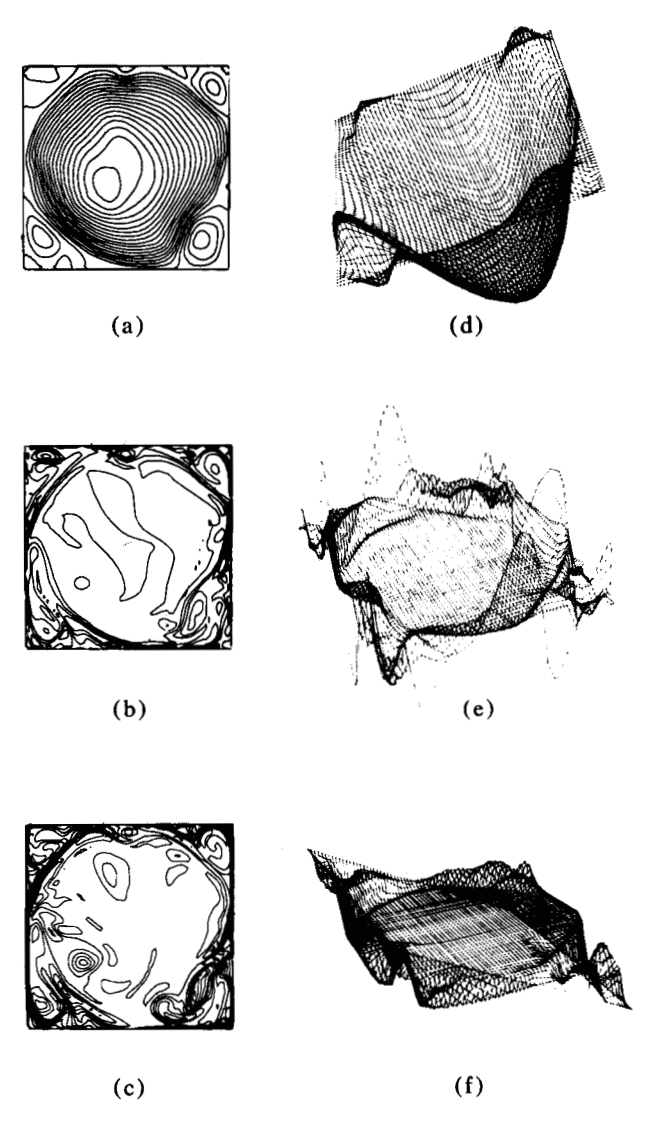


Figure 3 Single-circulation, high-Grashof-number flows. (a) Late-time streamline solution for $A=10^{12}$, $\sigma=1.0$. The plot increment $\Delta\psi=1.0$ ft²/sec. The separation streamline $\psi=0$ is given and is the reference contour. (b) Vorticity contours corresponding to Fig. 3(a). $\Delta\omega=10.0/{\rm sec.}~\omega$ maximum at the wall is 145.4. (c) Isotherms corresponding to Fig. 3(a). $\Delta T=0.5^{\circ}$ F. (d) Perspective view of Fig. 3(a). The corner nearest the observer is the lower left of Fig. 3(a). This is true for the remaining perspective views. (e) Perspective view of Fig. 3(b). (f) Perspective view of Fig. 3(c).

a reverse flow tendency which has its origin in a slight reversal in the horizontal temperature gradient.

In Fig. 1(b) one notes that the highest values of vorticity occur at the boundaries. The sign is opposite to the two buoyant vorticity extremals occurring near the vertical walls. This is the boundary layer vorticity which follows from our no-slip condition. The central extremal of vorticity is also of opposite sign to the main buoyant contributions. It also has its origin in buoyancy but here

in reverse to the main buoyant contributions. This reversed vorticity contributes to the attainment of steady flow in this range, along with the dissipation of frictional restraining forces. The latter mechanism is, of course, strongest at the boundaries. In the isotherms of Fig. 1(c), one clearly sees the slight reversal in horizontal temperature gradient at the center (the slant of the isotherms is downward to the right). Increased heat transfer relative to a nonfluid material is obvious from Fig. 1(c) in that the flow leads to high gradients in temperature at the vertical walls. Near the walls conduction is enhanced by the high gradients and in turn the flow in the center leads to exchange of warm and cold fluid through the convective process.

The results of Fig. 1 are not new; similar results have been obtained by Wilkes and Poots. To establish a point of departure from this earlier work we have compared a calculation of $A = 10^4$, $\sigma = 0.73$ with the results by Poots. The results are the same in all essentials in the visual sense of the solution. To further compare results we have numerically obtained the Fourier coefficients of our computed result for the disturbance temperature field [the linear gradient with $T_1 - T_0 = 10.0$ must be added to obtain the equivalent of Fig. 1(c)]. In Table 1 we compare the numerical coefficients with coefficients given by Poots. Differences in the results cannot be construed as error in the numerical results because Poots' solution is a cruder approximation. The differences in the second group of coefficients of Table 1 are puzzling and may be an error by Poots in recording the numbers. Consistencies for even smaller coefficients are good. Measured heat transfer at the cold wall as obtained by Poots is N = 1.706. We obtained N = 1.750 with the finite difference method, which should, of course, be far more accurate because many more modes are included than were possible in the modest calculations by Poots.

The sinusoidal range for $G \approx 10^7$ may cover as much as a decade of G. This range, like the steady state range, will have spatial symmetry. Asymmetry develops through fluid instabilities when roundoff errors relative to a line of symmetry differ. These instabilities grow exponentially and hence are manifest very quickly. While fluid instabilities are of interest in themselves and can be identified in the early stages of solution, we do not here analyze them. In general the instabilities follow upon one another, with the latter ones having such strong disturbance amplitudes that they are not traceable to well-defined equilibrium states. The advantage of the numerical solution is, of course, that these processes are accounted for without our need to know all the details, and we can concentrate on significant late-time flow features. Animations of the solutions have proved to be of great value in providing insight. The most important mechanisms in Fig. 2 ($A = 10^8$, $\sigma = 1$) are that boundary layer separ-

Table 1 Fourier coefficients of disturbance temperature distribution for $A = 10^4$, $\sigma = 0.73$ compared with Poots' calculations.

$Term(k_y, k_x)$	Poots	Finite difference
1.0	0.1077	0.1060
1, 2	-0.1875	-0.1868
2, 1	-0.1874	-0.1840
1, 4	0.0019	-0.0082
2, 3	0.0063	-0.0166
3, 2	-0.0107	0.0034
4, 1	-0.0314	-0.0359
1, 6	0.0017	0.0024
2, 5	0.0026	-0.0000
3, 4	-0.0004	-0.0014
4, 3	0.0016	0.0014
5, 2	0.0017	0.0024
6, 1	-0.0071	-0.0067
1, 8	0.0009	0.0010
2, 7	0.0018	0.0011
3, 6	0.0008	-0.0001
4, 5	0.0007	0.0006
5, 4	-0.0003	-0.0003
6, 3	0.0006	0.0002
7, 2	0.0008	0.0005
8, 1	-0.0018	-0.0015
1, 10	0.0001	0.0003
2, 9	0.0004	0.0004
3, 8	0.0003	0.0001
4, 7	0.0003	0.0001
5, 6	-0.0002	-0.0001
6, 5	0.0001	0.0002
7, 4	0.0001	-0.0001
8, 3	0.0003	0.0001
9, 2	0.0003	-0.0001
10, 1	-0.0006	-0.0005
1, 12		0.0001
2, 11		0.0001
11, 2		0.0000
12, 1		-0.0002

ation occurs and counter circulations to the main buoyant tendency can arise. When these do arise they influence the temperature field sufficiently to be enhanced by buoyant effects. In the transition range, steady state is probably impossible, although resonant effects might possibly be achieved through a highly critical choice of rectangular dimensions of the enclosure.

In Fig. 2(a) the separation streamline is given and counter circulation may be identified by tracing this streamline. Those circulations centered in regions toward the boundaries (exterior to the separation streamline) are counter circulations. The remaining significant centers of rotation are in the direction of the basic buoyant tendency. In the vorticity plots of Fig. 2(b) we note that the buoyant contribution from the vertical walls is confined to a very narrow vertical strip and this strip may be broken up into small concentrations. These move

upward along the heated wall much like air bubbles in water and give a wave character to the streamlines. Dominant characteristics in this range of A, even in the presence of the rapid time variation, are the strong circulations in the upper left and lower right corners. These circulations are enhanced by the rising and falling concentrations of buoyant vorticity from the heated and cooled walls. Boundary layer separation occurs immediately downstream from these dominant circulations. The counter circulations so developed usually migrate along the horizontal boundaries. Buoyant enhancement of the counter circulation is most likely in the vicinity of the lower left and upper right corners, where thermal boundary layers become stretched into plumes. In Fig. 2(c) such a plume is evident near the left side of the lower boundary.

In the included perspective view [Fig. 2(d)] the positive excursion of the streamfunction in the lower left corner is quite obvious. The vorticity plot [Fig. 2(e)] reveals a very strong shear layer at the vertical walls, where the buoyant vorticity and the wall generated vorticity are effective over a very short distance. A distinctive feature of Fig. 2(f) is the sharp temperature rise of the plume at the lower left boundary.

Measurement of the heat transfer in the transitional and upper range is difficult because the unsteadiness can lead to wide extremes (i.e., numerically we cannot measure transfer right at the wall). Long-term averages must be taken. Currently we are still in the process of dealing with these measurements along with necessary work that must be done on over-all data reduction. For the calculation of Fig. 2(a) $(A = 10^8, \sigma = 1)$ we estimate $N \approx 32.0$. Numerical programs to give late-time average heat transfer values have not been employed at this writing.

Finally we consider the last group (Fig. 3) in greater detail. The single circulation behavior of the high-Rayleighnumber flows is somewhat of a surprise because here the character of the flow is almost the same for a very wide range of values of the parameters. Quantitatively the flows remain different, particularly in the speed of circulation at late times or the rate at which the circulation speed increases from the initial no-flow state. In this range the viscous and conduction effects are essentially absent at the central region but intense at the boundaries. The results show dramatically why boundary layer theory has been so successful in many theoretical studies of fluid flow. While the unsteadiness far exceeds that of the transition range, it is almost entirely confined to a thin layer at the boundaries and to the corner regions. There is eccentricity in the flows that does not appear to diminish over the range of time covered by the calculations. An almost perfectly circular flow may be disrupted by migrating corner activity. Such a disruption may lead to increasingly eccentric flow but never a return to the type

of flow of the transitional range. Early transitional behavior from the no-flow initial condition does involve similar behavior to that of the transitional range flows.

In Fig. 3(d) we note that counter circulations to the main circulation are very limited. The apparent smooth appearance of this still shot is not indicative of the actual behavior. The activity of the flow is revealed in Figs. 3(e) and 3(f). The boundary generated vorticity is strong on all four walls and the entrainment of this vorticity into the corner regions leads to considerable activity there. A temperature greater than half the over-all temperature difference occurs within a short distance from the vertical walls. This phenomenon can account for the high heat transfer rates at high Grashof numbers. It occurs because the rapid circulation transports a thin column of warm or cold fluid in an overlapping manner to the cold and hot walls, respectively. Small extremals of vorticity [Fig. 3(b)] or hot spots of temperature [Fig. 3(c)] that occur on occasion in the central part of the flow have been timed to estimate a mean speed of the main circulation. In an 8-ft-square enclosure the circulation time is roughly 5 sec. This is not unreasonable but much work still needs to be done in comparing our results with experiment. It is uncertain to what extent the numerical result provides for the mixing that could occur in the turbulent flows observed in the laboratory.

Acknowledgments

The author wishes to acknowledge the assistance of Donald E. Schreiber [11], whose graphics programs for the IBM 2250 made it possible to reduce many numbers to meaningful pictures. Acknowledgment is also due William E. Langlois for his review and for his recommendations about the work and to Gary M. Giddings for the use of his marvelous three-dimensional display programs.

Appendix

In this appendix we describe the form of the convective approximation developed for the calculations. We shall give the form of the flux term in the x direction only but include various ranges of $\alpha = u\Delta t/\Delta x$ as indicated earlier. It must be remembered that the flux as given is only half of the required computation for a given mesh point. If the flux is added to the point on the right and subtracted from the point on the left, the length of computation can be reduced by half. Also the same convective program can be used for both vorticity and temperature if these variables are defined the same relative to the grid. The fluxes in the vertical direction may be inferred from those given here for the horizontal.

We define

$$\alpha_{i-\frac{1}{2},i} = \frac{u_{i-\frac{1}{2},i} \Delta t}{\Delta x} \quad \text{and} \quad \beta_{i-\frac{1}{2},i} = \frac{v_{i-\frac{1}{2},i} \Delta t}{\Delta y} ,$$

where

$$u_{i-\frac{1}{2},i} = (\psi_{i-1,i+1} + \psi_{i,i+1} - \psi_{i-1,i-1} - \psi_{i,i-1})/4 \, \Delta y$$

$$v_{i-\frac{1}{2},i} = (\psi_{i-1,i} - \psi_{i,i})/\Delta x.$$

If $|\alpha| < 0.09$ we use an upstream second-order approximation. We here write the central approximation terms with the understanding that if $\alpha > 0$, α is replaced by $(\alpha - 1)$ and i indices are reduced by 1. Further if $\alpha < 0$, α is replaced by $(\alpha + 1)$ and i indices are increased by 1. To make addition and subtraction of flux contributions possible, as previously mentioned, the powers of α must further be modified. For example α^2 must be replaced by $[(\alpha - 1)^2 - 1)] = \alpha^2 - 2\alpha$ so that Eq. (10) does indeed apply without a shift of index on the leading term of this equation. Cancellation of the appropriate linear terms (terms that do not contain α) can readily be verified for the difference forms here given. This, however, requires writing out the complete expression of both the flux into and out of the cell of interest.

Now define

$$S_{3,0} = T_{i-1,j} + T_{i,j},$$

$$D_{3,0} = T_{i-1,j} - T_{i,j},$$

$$S_{6,2} = T_{i-1,j+1} + T_{i,j+1},$$

$$D_{6,2} = T_{i-1,j+1} - T_{i,j+1}, \text{ and }$$

$$S_{7,4} = T_{i-1,j-1} + T_{i,j-1},$$

$$D_{7,4} = T_{i-1,j-1} - T_{i,j-1}.$$

Here the subscripts follow a layout as follows:

22	15	10	14	21
16	6	2	5	13
11	3	0	1	9
17	7	4	8	20
23	18	12	19	24

Now with index $i - \frac{1}{2}$ implied for α , β and F, we write

$$\begin{split} \frac{\Delta t}{\Delta x} F &= \frac{1}{2} \alpha S_{3.0} + \frac{1}{8} \alpha \beta (S_{7.4} - S_{6.2}) \\ &+ \frac{1}{2} \alpha^2 D_{3.0} + \frac{1}{12} \alpha \beta^2 (S_{7.4} - 2S_{3.0} + S_{6.2}) \\ &+ \frac{1}{6} \alpha^2 \beta (D_{7.4} - D_{6.2}) \\ &+ \frac{1}{8} \alpha^2 \beta^2 (D_{7.4} - 2D_{3.0} + D_{6.2}). \end{split}$$

For $0.09 \le |\alpha| < 0.5$ we use a fourth-order upstream expression and for $0.5 \le |\alpha| \le 1.0$ we use the average of the upstream and central expressions. Here again we give only the central difference expression. The same rules apply on replacement of α appropriately with

Table 2 Leading terms and differences of fourth-order approximation.

	В	X	
1 2	A ₁₁ α A ₂₁ α	$S_{3,0} \\ S_{11,1}$	
3	$A_{11}A_{11} \alpha \beta/2$	$S_{7,4} - S_{6,2}$	
4 5	$A_{11}A_{21} \ \alpha\beta/2 \ A_{21}A_{11} \ \alpha\beta/2$	$S_{18,12}-S_{6,2}-S_{15,10} \ S_{17,8}-S_{16,5}$	
6	$A_{21}A_{11} \alpha \beta / 2$ $A_{21}A_{21} \alpha \beta / 2$	$S_{23,19} - S_{17,8} + S_{16,5} - S_{22,14}$	
7 8	$A_{12} \alpha^2 \ A_{22} \alpha^2$	$D_{3,0} \ D_{11,1}$	
9	$A_{11}A_{12} \alpha \beta^2/3$	$S_{7,4} - 2S_{3,0} + S_{6,2}$	
10 11	$A_{11}A_{22} \alpha \beta^2/3 \ A_{21}A_{12} \alpha \beta^2/3$	$S_{18,12} - S_{7,4} - S_{6,2} + S_{15,10} \ S_{17,8} - 2S_{11,1} + S_{16,5}$	
12	$A_{21}A_{12} \alpha \beta^{7} / 3$ $A_{21}A_{22} \alpha \beta^{2} / 3$	$S_{17,8} - S_{11,1} + S_{16,5} + S_{22,14}$ $S_{23,19} - S_{17,8} - S_{16,5} + S_{22,14}$	
13	$2A_{12}A_{11} \alpha^2 \beta/3$	$D_{7,4} - D_{6,2}$	
14 15	$\begin{array}{ c c c c c c c c c c c c c c c c c c c$	$D_{18,12} - D_{7,4} + D_{6,2} - D_{15,10} \ D_{17,8} - D_{16,5}$	
16	$2A_{22}A_{21} \alpha^2 \beta/3$	$D_{23,19} - D_{17,8} + D_{16,5} - D_{22,14}$	
17	$A_{23} \ lpha^3$	X_2-X_1	
18 19	$A_{11}A_{23} \ lphaeta^3/4 \ A_{21}A_{23} \ lphaeta^3/4$	$\begin{matrix} X_4 - X_3 \\ X_6 - X_5 \end{matrix}$	
20	$A_{12}A_{12} \alpha^2 \beta^2/2$	$D_{7,4}-2D_{3,0}+D_{6,2}$	
21 22	$A_{12}A_{22} \ lpha^2eta^2/2 \ A_{22}A_{12} \ lpha^2eta^2/2$	$D_{18,12}-D_{7,4}-D_{6,2}+D_{15,10}\ D_{17,8}-2D_{11,1}+D_{16,5}$	
23	$A_{22}A_{22} \alpha^2 \beta^2/2$	$D_{23,19} - D_{17,8} - D_{16,5} + D_{22,14}$	
24 25	$3A_{23}A_{11} \alpha^3\beta/4 \ 3A_{23}A_{21} \alpha^3\beta/4$	$X_5 - X_3 \ X_6 - X_4$	
26	$A_{24} \alpha^4$	X_8-3X_7	
27 28	$A_{11}A_{24} \alpha \beta^4/5 \ A_{21}A_{24} \alpha \beta^4/5$	$\begin{array}{c} X_{10} - 3X_9 \\ X_{12} - 3X_{11} \end{array}$	
29 30	$\begin{array}{ c c c c c c c c c c c c c c c c c c c$	$X_{14} - X_{13} \\ X_{16} - X_{15}$	
31 32	$\frac{3A_{23}A_{12}}{3A_{23}A_{22}}\frac{\alpha^3\beta/5}{\alpha^3\beta/5}$	$\begin{array}{c} X_{11} - X_9 \\ X_{12} - X_{10} \end{array}$	
33 34	$\begin{array}{c} 4A_{24}A_{11} \ \alpha^4\beta/5 \\ 4A_{24}A_{21} \ \alpha^4\beta/5 \end{array}$	$\begin{array}{c} X_{15} - 3X_{13} \\ X_{16} - 3X_{14} \end{array}$	
35 36	$\begin{array}{c c} A_{12}A_{24} & \alpha^2\beta^4/3 \\ A_{22}A_{24} & \alpha^2\beta^4/3 \end{array}$	$\begin{array}{c} X_{21} - 3X_{20} \\ X_{23} - 3X_{22} \end{array}$	
37	$A_{23}A_{23} \ \alpha^3 \beta^3/2$	$X_{19}-X_{18}$	
38 39	$\begin{array}{c c} 2A_{24}A_{12} \ \alpha^4\beta^2/3 \\ 2A_{24}A_{22} \ \alpha^4\beta^2/3 \end{array}$	$\begin{array}{c} X_{22} - 3X_{20} \\ X_{23} - 3X_{21} \end{array}$	
40	$3A_{23}A_{24} \alpha^3 \beta^4/7$	$X_{28} - X_{27}$	
41	$4A_{24}A_{23} \alpha^4 \beta^3/7$	$X_{30} - 3X_{29}$	
42	$A_{24}A_{24} \alpha^4 \beta^4/2$	$X_{36} - 3X_{35}$	

Table 3 Coefficients of fourth-order approximation.

A_{11}	7/12	A_{21}	-1/12
A_{12}	15/24	A_{22}	-1/24
A_{13}	-1/12	A_{23}	1/12
A_{14}	-3/24	A_{24}	1/24

 $(\alpha - 1)$ or $(\alpha + 1)$ and shifting indices as previously indicated.

Define in addition to the above sums and differences

$$S_{15,10} = T_{i-1,j+2} + T_{i,j+2},$$

$$D_{15,10} = T_{i-1,j+2} - T_{i,j+2},$$

$$S_{18,12} = T_{i-1,i-2} + T_{i,i-2},$$

$$D_{18,12} = T_{i-1,i-2} - T_{i,i-2},$$

$$S_{11,1} = T_{i-2,j} + T_{i+1,j},$$

$$D_{11,1} = T_{i-2,i} - T_{i+1,i},$$

$$S_{16,5} = T_{i-2,j+1} + T_{i+1,j+1},$$

$$D_{16.5} = T_{i-2,i+1} - T_{i+1,i+1},$$

$$S_{17,8} = T_{i-2,j-1} + T_{i+1,j-1},$$

$$D_{17.8} = T_{i-2,i-1} - T_{i+1,i-1},$$

$$S_{22,14} = T_{i-2,i+2} + T_{i+1,i+2},$$

$$D_{22,14} = T_{i-2,j+2} - T_{i+1,j+2},$$

and

$$S_{23.19} = T_{i-2.j-2} + T_{i+1.j-2},$$

$$D_{23,19} = T_{i-2,j-2} - T_{i+1,j-2}.$$

We may now write, with index $i - \frac{1}{2}$ implied for α , β and F,

$$\frac{\Delta t}{\Delta x} F = \sum_{l=1}^{42} B_l X_l,$$

where the B's and X's are given in Table 2, and the numerical coefficients associated with the B's are given in Table 3.

References

- G. Poots, "Heat Transfer by Laminar Free Convection in Enclosed Plane Gas Layers," Quart. J. Mech. App. Math. 11, 257-273 (1958).
- J. O. Wilkes, "The Finite Difference Computation of Natural Convection in an Enclosed Rectangular Cavity," University of Michigan, Ph.D. Thesis, 1963.
- J. W. Deardorff, "A Numerical Study of Two-dimensional Parallel-Plate Convection," J. Atmos. Sci. 21, 419–438 (1964).

- 4. J. E. Fromm, "Numerical Solutions of the Nonlinear Equations for a Heated Fluid Layer," Phys. Fluids 8, 1757-1769 (1965).
- 5. K. Aziz, "A Numerical Study of Cellular Convection," Rice University, Department of Chemical Engineering, Houston, Texas (1965).
- 6. K. V. Roberts and N. O. Weiss, "Convective Differ-
- ence Schemes," *Math. Comput.* **20**, 272–299 (1966).

 7. J. E. Fromm, "Practical Investigation of Convective Difference Approximations of Reduced Dispersions,' in High-Speed Computing in Fluid Dynamics, International Union of Theoretical and Applied Mechanics Symposium, American Institute of Physics, New York, 1969.
- 8. G. I. Marchuk, "The Automatic Construction of Computational Algorithms," translated by G. J. Tee, Technical Report CS30, Computer Science Department, Stanford University, 1965.
- 9. O. Bunemann, "A Compact Non-Iterative Poisson

- Solver," SUIPR Report No. 294, Institute of Plasma Research, Stanford University, Stanford, California, 1969.
- 10. This technique was first employed by S. K. Jordan in his doctoral thesis, "Numerical Solutions for the Time-Dependent, Viscous, Incompressible Flow Past a Circle," Department of Aeronautics and Astronautics, Stanford University, 1970.
- D. E. Schreiber, "A Generalized Equipotential Plot-ing Routine for a Scalar Function of Two Variables," IBM Research Report RJ-499, 1968. This report is available on request from the Thomas J. Watson Research Laboratory library, Yorktown Heights, N. Y.

Received July 29, 1970

The author is located at the IBM Research Division Laboratory in San Jose, California.

J. E. FROMM